applied sciences

MDPI

Article

Feature-Aware Bidirectional Raster Path Planning for Robotic Line-Laser Scanning

Wei Zhang [1,*], Jikun Li [2], Zebang Gao [2] and Lina Hao [2]

[1] AVIC Changcheng Institute of Metrology and Measurement, Beijing 100095, China
[2] School of Mechanical Engineering and Automation, Northeastern University, Shenyang 110819, China; lijikun0924@163.com (J.L.)
* Correspondence: zhangw393@avic.com

Abstract

Robotic line-laser scanning of large components with spatially dispersed inspection features requires effective scanning-region identification and path organization to ensure measurement completeness. This study proposes a feature-aware bidirectional raster path-planning method based on discrete feature-point clouds. First, a region-growing algorithm is employed to divide the measurement surface into subregions according to geometric characteristics and surface-normal similarity. Subsequently, a two-level partitioning strategy is introduced to identify scanning execution units containing target feature points. Local bidirectional scanning paths are generated within the retained execution units to improve the coverage of relevant measurement features. Finally, a greedy endpoint-selection strategy is adopted to organize the scanning sequence and connect the local paths. An aircraft nose-frame flange is used to evaluate the proposed method. Under the adopted geometric coverage criterion, the scanning coverage rate increases from 84% using the conventional bidirectional raster method to 97% using the proposed approach, representing an improvement of 13 percentage points. The results demonstrate the potential of feature-aware region partitioning to reduce unscanned target areas and improve the completeness of geometric scanning coverage. The study provides a path-planning framework for robotic line-laser inspection of large components. Further validation of robot-level reachability, collision avoidance, and practical scanning performance is required.

Keywords: robotic inspection; coverage path planning; feature-based segmentation; line-laser scanning; geometric path generation

Check for updates

Academic Editor: DaeEun Kim

Received: 10 October 2026
Revised: 27 October 2026
Accepted: 29 October 2026
Published: 6 November 2026

Copyright: © 2026 by the authors. Licensee MDPI, Basel, Switzerland. This article is an open access article distributed under the terms and conditions of the Creative Commons Attribution (CC BY) license.

1. Introduction

1.1. Research Context

As large and complex components become more common in aerospace, shipbuilding, and advanced equipment manufacturing, dimensional inspection must meet increasingly demanding requirements for measurement efficiency, data completeness, and automation. Line-laser scanning is non-contact, enables rapid data acquisition, and is well suited to measuring complex surfaces. It has therefore been increasingly adopted for the automated inspection of large components. However, such components often have extensive dimensions, dispersed local features, and complex surface geometries. Applying a fixed scanning area or planning a path that covers the entire area can generate substantial redundant scanning, increase measurement time, and reduce the continuity of robot motion.

The quality of measurement path planning directly affects inspection completeness, measurement accuracy, and operational efficiency [1]. In robotic laser scanning, path planning is therefore essential to automated, efficient, and accurate measurement. Existing studies on large and complex components, including aircraft structural parts, wings, and panels, have addressed path optimization, scanner pose optimization, scanning sequence optimization, and surface tracking.

1.2. Recent Related Works

Lin [2] investigated the coupled effects of scanning depth, in-plane angle, and out-of-plane angle on the systematic error of a robot-mounted T-Scan laser scanner. They first established a bilinear predictive model relating scanning parameters to systematic error through experimental calibration. Using this model as the objective function, they applied particle swarm optimization to determine the optimal scanning pose for each local surface under constraints on depth of field, scanning width, and receiving angle. They then formulated the scanning sequence for spatially dispersed features as a traveling salesman problem (TSP) and used an improved Hopfield neural network to minimize non-scanning travel. Their approach jointly improved local measurement accuracy and overall scanning efficiency.

To address frequent pose adjustments and redundant travel when scanning the large, continuous curved surfaces of wing panels, Xiaoxiang Ai [3] proposed a path-planning method combining least-squares-based adaptive grouping with global optimization using a genetic algorithm. The method adopts raster scanning as its overall strategy and groups discrete surface samples with similar normal vectors, allowing each group to be covered by a set of continuous, smooth scanning planes. This reduces the number of scanner pose adjustments. The spatial poses of the scanning planes are then optimized with a genetic algorithm to minimize total path length while satisfying constraints on scanner inclination, depth of field, and scanning width. Experiments showed an approximately 14.4% improvement in scanning efficiency compared with conventional straight-line scanning.

An'an Zhao et al. [4] addressed the limited adaptability of a single planning strategy when multiple feature types, such as grooves, ribs, holes, and stiffeners, are distributed across an aircraft panel. They proposed an adaptive path-planning algorithm based on region segmentation. Starting from a triangular mesh of the part, the algorithm segments the surface using the dihedral angles and normal-vector angles between adjacent triangles, and extracts feature surfaces whose normals are approximately perpendicular to the scanning reference vector. Principal component analysis (PCA) is then used to project each feature surface onto a local two-dimensional plane for path planning. The resulting paths are mapped back into three-dimensional space and offset by a specified angle to obtain the final scanning trajectories. The authors also presented full and simplified segmentation strategies for models with extensive curved surfaces and CAD models with clearly defined edges, respectively.

Recent studies have investigated robotic inspection planning from several complementary perspectives. Glorieux et al. [5] examined targeted viewpoint sampling for robotic free-form surface inspection. Liu et al. [6] incorporated measurement uncertainty into coverage path planning for robotic quality inspection. Jia et al. [7] combined adaptive surface sampling, scanning-attitude calculation, viewpoint planning, and bidirectional scanning. Chen et al. [8] considered scanning-path length and orientation changes within a dynamic-programming formulation. Chen et al. [9] investigated region segmentation and global inspection-sequence optimization for robotic line scanning, while Pi et al. [10] addressed curvature-adaptive viewpoint generation and robot scanning-posture optimization.

Measurement-aware planning also requires attention to sensor configurations and measurement quality. Sadaoui et al. [11] developed an automatic path-planning approach for laser plane sensors that considers scanning angle, scanning distance, measurement quality, accessibility, visibility, and collision handling. Their implementation was evaluated using a laser sensor mounted on a coordinate measuring machine. Focusing on T-SCAN, Feng et al. [12] investigated measurement-posture modeling, scanning-path planning, and measurement-station planning for complex features. These studies indicate that the geometric organization of scanning paths should be distinguished from verification of measurement quality and practical feasibility.

These studies demonstrate that region segmentation, viewpoint selection, raster scanning, and sequence optimization are established components of inspection planning. The present study focuses on a narrower geometric-planning problem: selecting scanning execution units for spatially dispersed target features and ordering their local paths. Its methodological emphasis is the combination of feature-occupancy-based execution-unit selection and reversible endpoint-based region connection. The individual computational tools are not claimed as new algorithms.

The available example illustrates the planning workflow. It does not establish quantitative superiority over recent methods or demonstrate robot-level executability.

1.3. Limitations of Existing Methods

Taken together, these studies show progression from single-objective to coordinated multi-objective optimization, from assumptions of continuous surfaces to methods suited to complex components with multiple feature types, and from simple raster scanning to region segmentation and global sequence optimization. They provide a foundation for robotic line-laser scanning. Nevertheless, conventional methods that plan from the overall boundary of a measurement area may still scan regions without relevant features. When the area is divided into multiple subregions, the order of transitions between them can substantially affect travel distance and scanner pose adjustments. For a manipulator-mounted scanner, long paths within individual regions and poorly planned transitions may also reduce path executability and process stability.

1.4. Novelty

To address these issues, this study uses a discrete point cloud of a large component as its research object. Building on measurement-constraint modeling and region partitioning, it introduces a segmentation strategy based on the spatial distribution of feature information and proposes an improved bidirectional raster-scanning path-planning method. The method distinguishes effective measurement regions from areas that do not require measurement, generates local bidirectional raster paths only in regions containing relevant features, and uses a greedy strategy to optimize the order of transitions between subregions. These steps are intended to avoid assigning scanning passes to empty projected cells and to organize transfers between retained local paths. The present evaluation focuses on geometric target coverage. Effects on total travel distance, non-scanning travel, and execution time are not quantified.

1.5. Objective of the Study

The objective of this study is to formulate a geometric scan-path generation workflow for large components with dispersed target features. The present scope includes feature-based execution-unit selection, local raster-path generation, and region ordering. The present study evaluates geometric target coverage for the selected example. Path-length optimization, execution-time assessment, and robot-level validation are outside its scope.

1.6. Main Contributions

The main contributions are as follows:

(1) a geometric planning formulation for selecting execution units containing target feature points;
(2) integration of local bidirectional raster paths with reversible endpoint-based region ordering; and
(3) an illustrative application to an aircraft nose-frame flange, accompanied by an explicit statement of the evidence and validation limitations.

The remainder of this paper is organized as follows. Section 2 presents the measurement model and geometric planning method. Section 3 describes the available illustrative results. Section 4 discusses limitations and future work. Section 5 presents the conclusions.

2. Materials and Methods

The planning configuration considered in this study comprises a line-laser scanner intended to be carried by an AUBO-i10 manipulator. The manipulator is identified as a target implementation platform. Its inverse kinematics, workcell placement, joint motion, and collision status are not evaluated in the present study.

Depending on the geometry of the component, a line-laser scanner can operate in two measurement modes [13], as illustrated in Figures 1 and 2. In surface-following measurement, the scanner continuously adjusts its pose to follow the measured surface while maintaining an approximately constant stand-off distance, thereby accommodating changes in surface curvature. In fixed-axis measurement, the scanner does not move along one direction during scanning. Because this study concerns large components with long scanning paths and measurement cycles, fixed-axis measurement is adopted to reduce scanner pose adjustments and improve measurement efficiency.

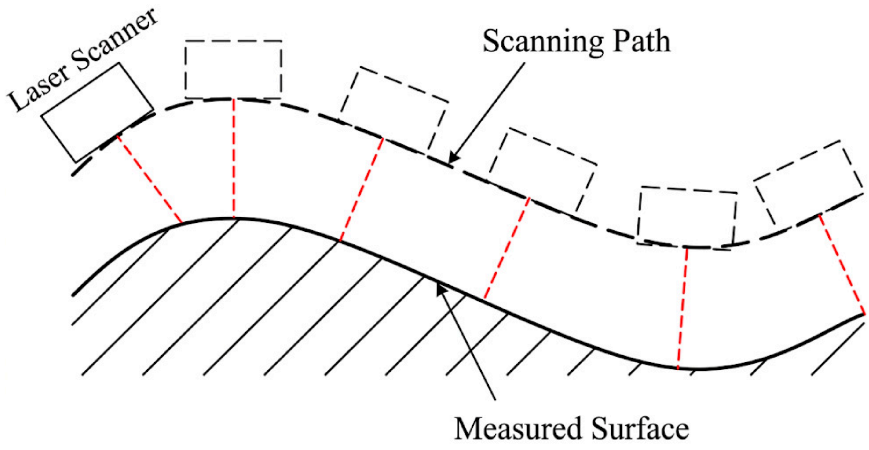


Figure 1. Surface-following measurement.

After selecting the measurement mode, the proposed workflow proceeds in three stages. First, a measurement-constraint model is established for the Leica T-Scan 5-line-laser scanner. Second, a region-growing algorithm is used to cluster the point cloud representing the component's geometric features, partition the measurement area, and generate scanning viewpoints. Finally, the scanning viewpoints are connected using the proposed improved bidirectional raster-scanning path-planning algorithm to obtain the final scanning path. The workflow is shown in Figure 3.

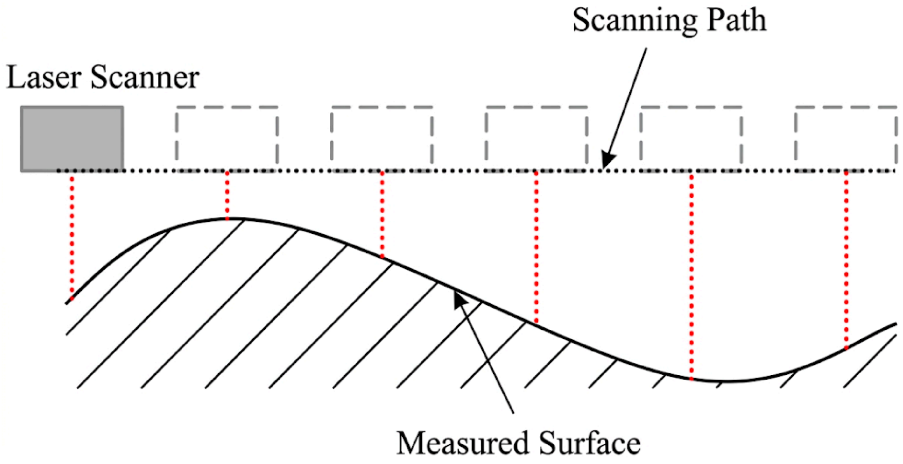


Figure 2. Fixed-axis measurement.



Figure 3. Basic measurement procedure flowchart.

2.1. Improving the Bidirectional Line-by-Line Scanning Path-Planning Method

Building on the overall process from Section 2, we go into detail about the planning method.

2.1.1. Scanner Measurement Constraint Model

During scanning, measurement quality depends not only on the sensor's internal parameters and environmental conditions, but also on parameters associated with the scanning strategy, particularly those used to define the measurement path [14]. Previous studies [15,16] have shown that scanning angle and scanning distance strongly affect measurement accuracy and quality. Accordingly, to obtain accurate scan data while improving efficiency, this study establishes a measurement-constraint model based on these two factors.

The measurement-constraint model is illustrated in Figure 4. The laser scanner emits a probing beam from position L, forming a field of view with L as its vertex and an angular extent of σ. B_i denotes the angular bisector of the boundaries of the emitted beam. P_i is the ith measurement point on the surface, and N_i is its corresponding surface normal vector [17]. The symbols l_n and l_f denote the near and far working-distance limits, respectively. The symbol l_s denotes the nominal stand-off distance adopted for geometric path construction. The scanning path must satisfy the following constraints:

1. Measurement inclination angle. Let N_i denote the outward unit normal at surface point P_i and let d_i denote the unit vector directed from P_i toward the scanner position L. The inclination angle θ is defined between these two vectors. According to the principle of optical triangulation, the optimal angle is obtained when the incident direction is collinear with the surface normal, providing an inclination angle of zero [18]. In practice, the required measurement accuracy can also be achieved at a nonzero inclination angle, provided that it does not exceed a specified threshold γ: $\theta \leq \gamma$

$$d_i^T \cdot N_i \geq \cos(\gamma), \tag{1}$$

$$d_i = (L - P_i)/\|L - P_i\|. \tag{2}$$

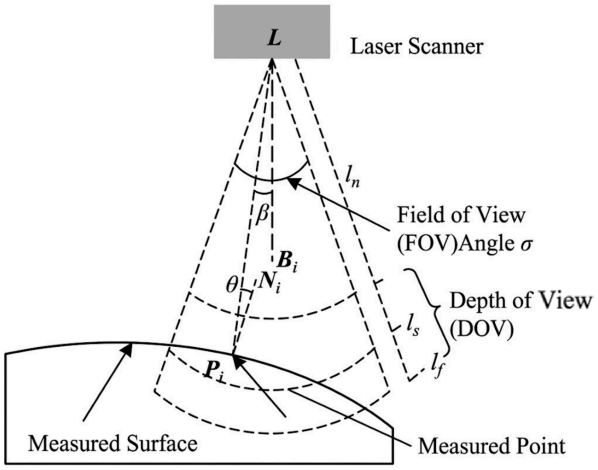


Figure 4. Scanner measurement constraint model.

2. Field-of-view width (FOV). Let b be the unit field-of-view axis directed from the scanner toward the inspected region. Since the viewing ray is $-d_i$, the half-field-of-view constraint is provided by Equation (2). Each measurement point P_i must lie within the effective length of the laser stripe in the scanner's field of view. Because the distance from the scanner to each point varies, the effective stripe length also varies with distance. Each point must therefore satisfy the field-of-view constraint:

$$(-d_i)\cdot B_i \geq \cos(\sigma/2), \tag{3}$$

where σ is the field-of-view angle, a fixed parameter of the laser scanner.

3. Depth of view (DOV). Each measurement point on the surface must lie within the scanner's specified working-distance range:

$$l_n \leq \|L - P_i\| \leq l_f, \tag{4}$$

where the limits correspond to the far and near working distances; the remaining parameters describe the scanner's viewing distance and measurement depth.

4. Visibility and collision constraints. The incident scanning direction must not be occluded by the component, and the scanner must remain collision-free throughout the scan.

2.1.2. Scan Viewpoint Planning Based on Region Growing Algorithm

To ensure that the laser scanner acquires valid measurement data at the required accuracy, the scanning process must satisfy its measurement-constraint model. First, the angle between the surface normal at each measurement point and the incident laser beam must not exceed the specified threshold (a Leica T-Scan 5 scanner, Leica Geosystems, Heerbrugg, Switzerland, is used in this study; $\gamma = 10°$). Second, each measurement point must lie within the scanner's depth-of-view range ($[l_n \sim l_f]$) to ensure data reliability. Using the coordinates and normal vectors of feature points extracted from the large component, this study applies region growing to partition its geometry. The complex surface is divided into approximately planar subregions with consistent normal vectors. Each subregion is assigned a representative normal vector; its opposite direction defines the incident laser direction for that region, allowing the scanner to measure the entire subregion from a single pose.

Region growing [19] is a conventional segmentation method that starts from a seed point and iteratively adds neighboring points that satisfy a predefined similarity criterion

until a termination condition is met. The result is a set of regions with internally consistent features. In this study, the method is used to partition the measurement area geometrically. Seed points are selected according to curvature, normal-vector angles serve as the growth criterion, and scanning viewpoints are planned subject to the depth-of-view constraint [20]. The procedure is described below.

To obtain smooth, non-overlapping regions, the point with the lowest curvature in the measurement area is selected as the initial seed. Because this point lies in a relatively flat part of the surface, growing a region from it can reduce the number of resulting subregions while helping to maintain their smoothness. First, curvature is estimated for the points in the input cloud, and the points are sorted in ascending order of curvature. Region growth then proceeds according to normal-vector similarity: a neighboring point is added to the current region when the angle between its surface normal and the incident laser direction satisfies the specified angular threshold. Growth of the current region is considered complete when no neighboring points satisfy the growth criterion, the number of points in the region no longer changes, and the angle between every point normal in the region and the region's mean normal does not exceed the threshold.

The input is the set $C = \{D_1, D_2, D_3 \ldots D_N\}$, $D_k = (p_k, n_k)$ of feature points extracted from the large component. Each feature point contains its coordinates along the X, Y, and Z axes of the world coordinate system and the corresponding three components of its normal vector. The region-growing method partitions C into M subsets for optimal scanning-viewpoint planning. The algorithm workflow is shown in Figure 5, and its steps are detailed below. Here, N is the number of input feature points, p_k is the point position, and n_k is its unit normal. The number of regions is denoted separately by M.

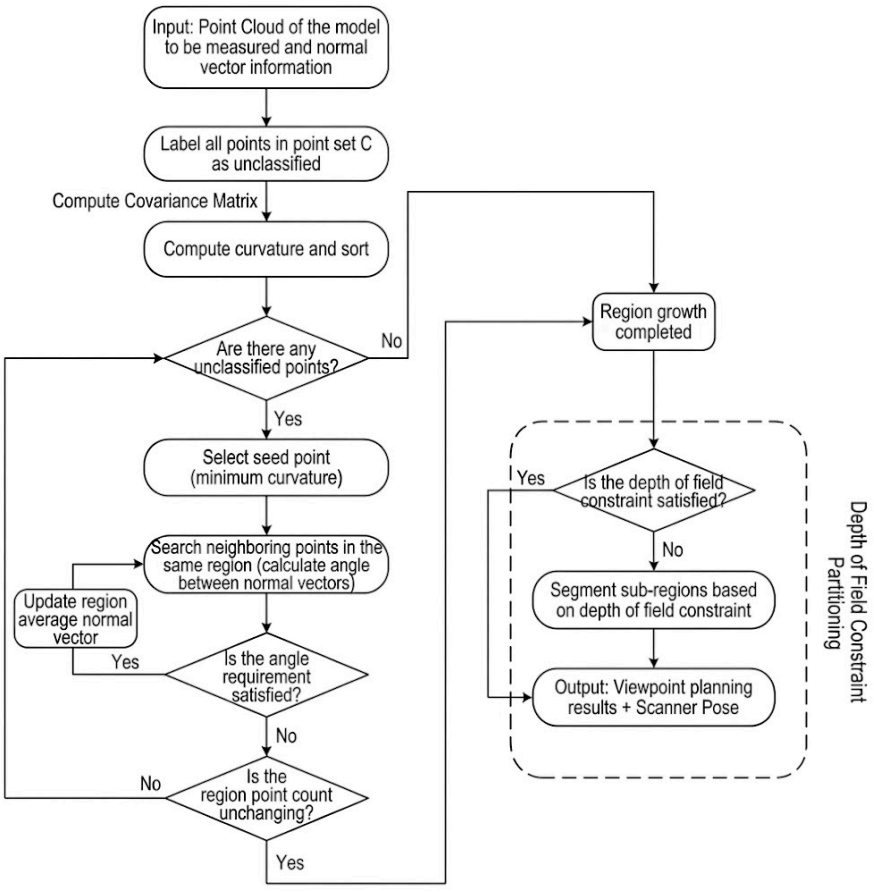


Figure 5. Flow of the laser scanner viewpoint planning algorithm based on the region-growing method.

2.1.3. Scan Path Planning Based on an Improved Bidirectional Row-Cutting Strategy

Section 2 selected the fixed-axis measurement mode, in which the laser scanner maintains a fixed offset from the measured surface and scans by translating within a plane. Depending on the path pattern, raster scanning can be performed either unidirectionally or bidirectionally. Compared with bidirectional scanning, unidirectional scanning produces more non-scanning travel within the same measurement region and therefore requires more time, as shown in Figure 6. Bidirectional raster scanning offers higher measurement efficiency. Accordingly, considering measurement efficiency, measurement accuracy, and the number of scanner pose adjustments, this study adopts bidirectional raster scanning for data acquisition.

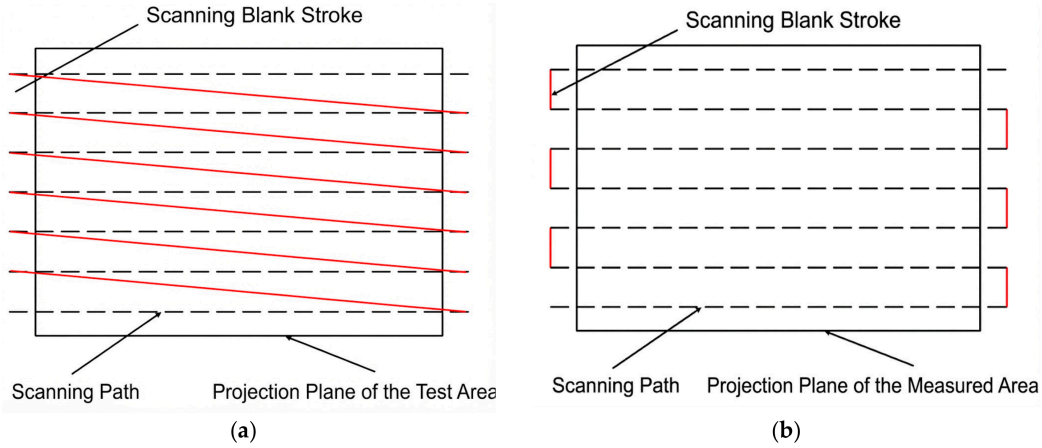


Figure 6. Scan strategy analysis. (**a**) Unidirectional row-by-row scanning strategy; (**b**) bidirectional row-by-row scanning strategy.

The overall scanning path-planning process comprises two stages: viewpoint planning and path planning. Together, they are essential to the efficiency and accuracy of laser scanning for large components and to the feasibility of robot-arm execution. In Section 2.1.2 viewpoint planning partitioned the component's geometric features into measurement regions and determined the optimal scanner pose for each region. However, discrete viewpoints alone cannot guide a scanning operation; they must be connected to form continuous, controllable paths. Conventional raster-scanning algorithms also have limitations in efficiency and compatibility with robot-arm execution. This section therefore improves the basic bidirectional raster-scanning algorithm and proposes an improved path-planning method.

The following subsections describe the implementation of the proposed method. The representative orientation assigned to each region is used to construct candidate scanning paths. This regional approximation does not establish that every surface point satisfies the inclination-angle and working-distance constraints along the complete trajectory. The set of feature-point information for the ith region is denoted by $F_i = \{F_{i,1}, F_{i,2}, F_{i,3} \ldots F_{i,n}\}$, $i = 1, 2, 3, \ldots, n$.

1. Mapping to a Two-Dimensional Plane

The points in each region are mapped to a two-dimensional plane by projection. The plane's normal is defined as the mean unit normal obtained from region growing, $\overline{n_{s_i}} = (n_x, n_y, n_z)$, where $\|\overline{n_{s_i}}\| = 1$. The centroid of the points in the region is used as the plane's center, $O_{avg} = (1/n)\sum_{k=1}^{n} F_k$. Here, n denotes the number of feature points in the current region. The centroid represents the arithmetic mean of all these points. The summation is intended to include each feature point in the region once, with k serving as the dummy summation index. Two basis vectors, μ_i and v_i, are then determined to obtain the projected coordinates of the discrete points [21].

First, principal component analysis (PCA) is applied to the discrete point set. Its first principal component is denoted by μ_{PCAi}. Subtracting the component of this vector along the plane normal yields the first in-plane basis vector:

$$\mu_i = \mu_{PCAi} - (\mu_{PCAi} \cdot \overline{n_{s_i}}) \overline{n_{s_i}}. \tag{5}$$

Next, μ_i is normalized and combined with $\overline{n_{s_i}}$ to obtain the second in-plane basis vector:

$$v_i = \overline{n_{s_i}} \times \frac{\mu_i}{|\mu_i|}. \tag{6}$$

Finally, the projected coordinates $F_i^{2D} = \left(x_i^{2D}, y_i^{2D}\right)$ of point F_i are calculated as

$$\begin{cases} x_i^{2D} = \left(F_i - O_{avg}\right) \cdot \mu_i \\ y_i^{2D} = \left(F_i - O_{avg}\right) \cdot v_i \end{cases}. \tag{7}$$

2. Determination of an Oriented Bounding Box

For each two-dimensional projected point set, principal component analysis (PCA) is used to construct an oriented bounding box (OBB). Compared with a conventional axis-aligned bounding box, the OBB more closely encloses the projected region and reduces scanning paths over areas outside it. First, the covariance matrix $cov[B, B]$ is calculated to describe the distribution of points in the two-dimensional plane:

$$cov[B, B] = \begin{bmatrix} \sigma(x,x) & \sigma(x,y) \\ \sigma(x,y) & \sigma(y,y) \end{bmatrix}. \tag{8}$$

The variance and covariance terms are calculated as shown in Equation (8). Eigenvalue decomposition of the covariance matrix then yields eigenvalues λ_1 and λ_2, where $\lambda_1 > \lambda_2 > 0$ and their corresponding eigenvectors u_1 and u_2.

The eigenvector u_1, associated with the larger eigenvalue, defines the direction of the OBB's long axis; u_2, associated with the smaller eigenvalue, defines its short axis. A new planar coordinate system is established for each region, with u_1 and u_1 as its X and Y axis directions, respectively, and the region's centroid as its origin. The points are projected onto these two axes, and the extreme projected coordinates are used to determine the box vertices, completing the OBB construction [22].

$$\begin{cases} \sigma(x,x) = \frac{1}{n}\sum_{i=1}^{n}\left(x_i^{2D} - \overline{x}^{2D}\right)^2 \\ \sigma(x,y) = \frac{1}{n}\sum_{i=1}^{n}\left(x_i^{2D} - \overline{x}^{2D}\right)\left(y_i^{2D} - \overline{y}^{2D}\right) \\ \sigma(y,y) = \frac{1}{n}\sum_{i=1}^{n}\left(y_i^{2D} - \overline{y}^{2D}\right)^2 \end{cases}. \tag{9}$$

In Equation (9), $\overline{x}^{2D}$ and $\overline{y}^{2D}$ denote the arithmetic means of the projected x- and y-coordinates, respectively, calculated over all n feature points in the current region. The quantities x_i^{2D} and y_i^{2D} are the projected coordinates of the ith feature point. Thus, the variance and covariance terms describe the spatial distribution of the projected points within that region.

3. Region Segmentation Based on Feature Information

The proposed method extends conventional bidirectional raster scanning by introducing a two-level grid partition. Each original clustered region is first divided into large cells that define task-level subregions. These are then subdivided into smaller cells that serve as scanning execution units. Small cells containing no projected feature points are removed. This partition accounts for both the laser scanner's effective scan-line width and the robot

arm's working range from a single setup, enabling finer region segmentation while reducing redundant paths. The side length of each large cell is selected according to the AUBO robot arm's working range and can be adjusted for the task; it is set to 250 mm in this study. The dimensions of the small cells are matched to the scanner's effective scan-line width. After empty cells are removed, every retained cell contains at least one projected feature point, and each large cell can be measured from a single robot setup. For feature points across grid boundaries, a dual-cell assignment strategy is used, meaning boundary features are included in both adjacent cells to avoid missing narrow features or sparsely distributed points at the edges of the grid.

The archived example uses nominal task-cell and execution-cell dimensions of 250 mm and 130 mm, respectively. Both types of parameters are chosen based on hardware specs and experience and haven't been automatically optimized. These values are reported as settings of the example and are not established as optimal or as guarantees of robot reachability and complete coverage. The long axis is aligned with a direction that supports smooth motion of the robot end effector. If the dimensions of an original clustered region do not meet these partitioning rules, priority is given to satisfying the scan-line-width requirement along the short axis, and the region is expanded as needed. The entire two-dimensional projected region is thereby divided into N rectangular task-level subregions. The relationship between nominal cell dimensions, partial boundary cells, and effective scanning width requires further specification and evaluation. No parameter-sensitivity analysis is available in the present study.

Each task-level subregion is then divided into m smaller scanning execution units according to the scanner's effective scan-line width. Units containing no projected feature points are removed, yielding the final set of scanning execution units.

4. Generation of Bidirectional Raster-Scanning Paths in the Two-Dimensional Plane

To ensure complete measurement of each region, the planned path must cover every retained scanning execution unit. The four vertices and the lengths of the long and short sides of each unit are determined from its two-dimensional coordinates. To reduce scanner pose adjustments, the X axis of the execution unit is selected as the scanning direction. Because each unit has already been sized according to the scanner's effective scan-line width, it requires only one scanning pass; thus, $n_s = 1$.

The start and end points of this pass are then determined in the two-dimensional plane. To maintain measurement quality near the surface boundary and ensure full coverage without excessive path extension, the scan line is extended beyond the unit's boundaries. Since $n_s = 1$ the scanner travels along the X axis once. The path is centered across the unit's width, giving the start point P_s and end point P_e as

$$P_s = \left(x_{min} - \delta d_x, \frac{y_{max} + y_{min}}{2} \right), \tag{10}$$

$$P_e = \left(x_{max} + \delta d_x, \frac{y_{max} + y_{min}}{2} \right). \tag{11}$$

Here, x_{min} and x_{max} denote the minimum and maximum x-coordinates of the current scanning execution unit, respectively, in the local two-dimensional planning coordinate system. Similarly, y_{min} and y_{max} denote its minimum and maximum y-coordinates. These bounds refer to the current execution unit rather than the entire component. The term $(y_{max} + y_{min})/2$ specifies the transverse midpoint at which the scanning segment is placed. The parameter δ is the boundary extension coefficient, and δdx denotes the specified extension distance.

5. Global Path Planning

After raster-scanning paths have been generated for the individual subregions, the local paths remain disconnected. Global path planning is therefore required to determine the order in which the regions are measured and to connect their local paths into a complete measurement trajectory. The objective is to reduce travel between regions and the time spent adjusting the robot arm's pose, thereby improving overall measurement efficiency.

A simple connection strategy joins the end of one regional path directly to the start of an adjacent regional path. This can produce long non-scanning movements between regions and substantially increase measurement time. To address this issue, a greedy global path-planning algorithm is adopted [23]. At each step, the algorithm selects the endpoint of an unvisited region that is closest to the current path endpoint as the next destination.

Specifically, the start and end points of each regional scanning path are treated as candidate connection points. Planning begins at the start point of a selected region. After its local path has been traversed, the nearest endpoint of an unvisited region is selected as the next entry point. The process continues until every region has been measured, producing a connected global scanning path. The algorithm workflow is shown in Figure 7.

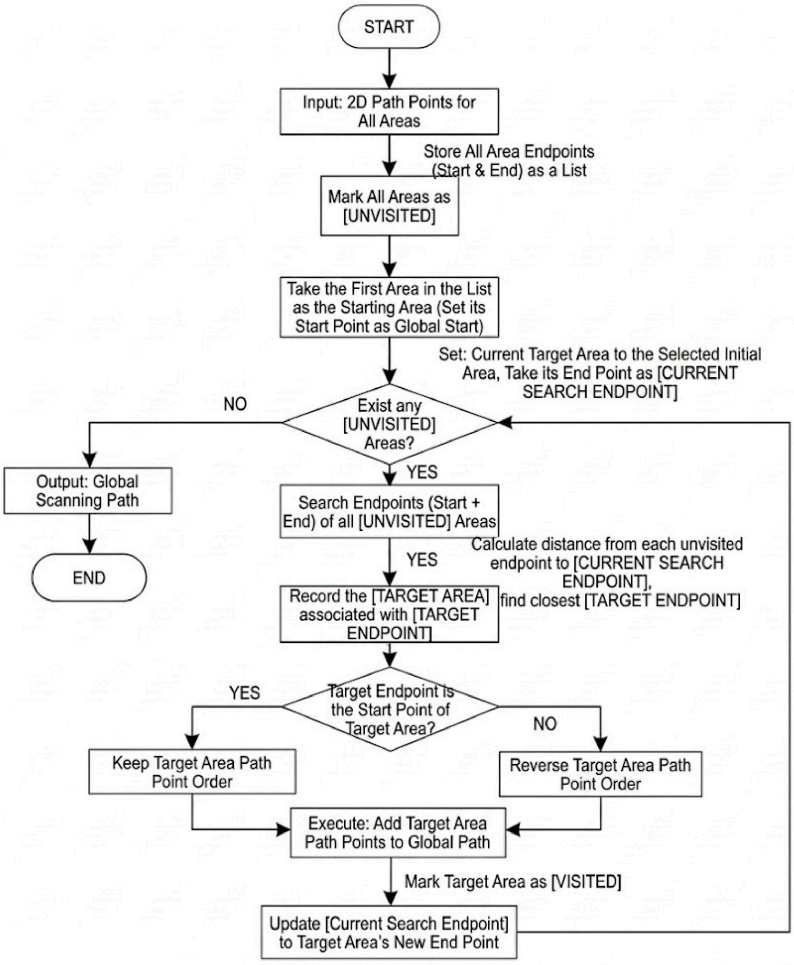


Figure 7. Global path planning algorithm process.

The global path-planning algorithm takes the measurement path points generated after task-level partitioning as its input. The ordered path points for each region are stored in a separate list, and these regional lists form a nested list.

An initial region is selected, and the start point of its local scanning path is used as the start of the global path. From the end point of that region's path, the algorithm searches for

the nearest start or end point among the unvisited regions. If the nearest point is the start of the selected region's path, its path-point order is retained. If the nearest point is the end, the entire path-point order is reversed, so that this point becomes the region's entry point.

The search then continues from the end of the newly ordered regional path. The nearest-endpoint search and, where necessary, path reversal are repeated until no unvisited regions remain. The ordered regional paths are then connected to form the global scanning path.

The nearest-endpoint rule is a heuristic and does not guarantee the minimum total connection length. Its result depends on the initial region and local endpoint choices. For large components that are fragmented into sub-regions and numerous in quantity, metaheuristic algorithms aimed at TSP (like genetic algorithms, simulated annealing, etc.) can bring a high computational cost. Greedy strategies strike a balance between planning efficiency and path optimization, making them more suitable for on-site quick measurement planning scenarios.

6. Mapping to Three-Dimensional Space

After the scanning paths have been planned in their respective two-dimensional planes, the path points are mapped from the local two-dimensional coordinate systems back to the original three-dimensional coordinate system. This inverse coordinate transformation produces a sequence of three-dimensional base path points from the planned two-dimensional path points, as expressed in Equation (12).

$$P_i^{base} = O_{avg} + x_i^{2D} \cdot \hat{\mu}_i + y_i^{2D} \cdot \hat{v}_i. \tag{12}$$

Here, O_{avg} is the center point of the area; the remaining vectors are the unit vectors along the first and second basis directions of the projection plane, respectively.

To maintain measurement accuracy and imaging quality, all three-dimensional base path points in each region are then offset along that region's mean normal vector. The offset is set to the scanner's optimal stand-off distance, yielding the final sequence of three-dimensional scanning path points, as expressed in Equation (13). Candidate scanner positions are obtained by offsetting the reconstructed planar path along the regional mean normal by the nominal stand-off distance. This operation defines a geometric path but does not, by itself, verify pointwise working distance, incidence angle, visibility, or collision avoidance on the actual surface.

$$P_i^{3D} = P_i^{base} + l_s \cdot \overline{n_{s_i}}. \tag{13}$$

Pointwise measurement-constraint verification and correction of infeasible path segments are required before practical execution and are included in future work.

3. Results

Feature-based cell selection changes where local scanning passes are assigned. Cells containing no projected feature points are excluded from local scan generation, while retained paths are ordered using endpoint proximity. These are structural properties of the workflow. Their effects on complete three-dimensional coverage and robot cycle time cannot be determined from the available visualizations.

Finer partitioning may reduce scanning over non-target areas but can also increase the number of local segments and transfers. Similarly, a short Euclidean connection may require a longer feasible robot motion. The geometric metrics for the selected configuration are compared in Table 1. However, the effects of partition dimensions, alternative connection strategies, and robot-level motion constraints have not been systematically evaluated.

Table 1. Geometric coverage comparison for the nose-frame flange case study.

Indicator	Original Planning Algorithm	Improved Scan Path-Planning Algorithm
Scanning coverage rate/%	84	97
Uncovered target rate (%)	16	3
Total scanning path length/mm	14,346	18,752
Number of scanning regions	2	2
Number of scanner pose adjustments	2	2

The flange surface of the nose frame was used as an example. Feature extraction yielded 65,816 feature points and their corresponding normal vectors. After parameter tuning, the region-growing algorithm was configured with a minimum cluster size of 50 points, a maximum cluster size of 8000 points, 80 neighbors for neighborhood search, a normal-vector angle threshold of 5°, and a curvature threshold of 0.01. The resulting two scanning-viewpoint regions are shown in Figure 8. The red region is Cluster 01, and the green region is Cluster 02.

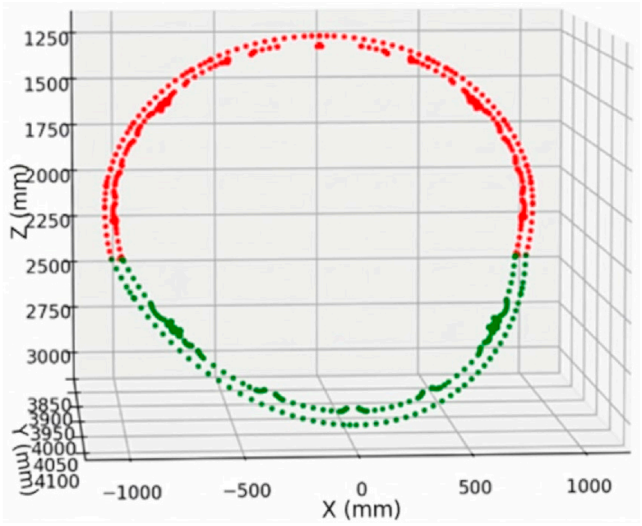
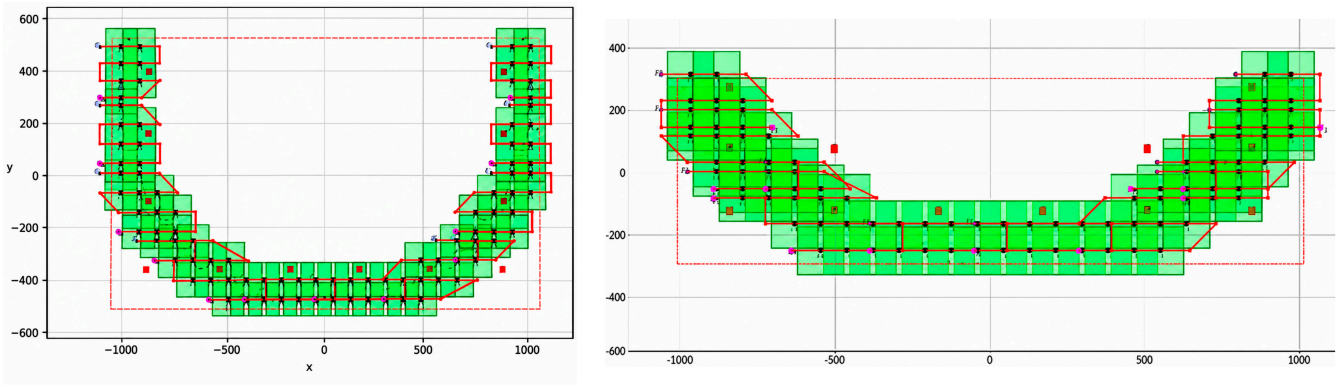


Figure 8. Clustering results based on the region growth algorithm.

Following clustering, the flange-surface region was used to demonstrate two-dimensional path planning. The side length of the large cells used for feature-based partitioning was set to 250 mm, while the small-cell side length was set to 130 mm with reference to the T-Scan 5's scan-line width to obtain a compact path without coverage gaps. The result is shown in Figure 9. The green areas indicate the secondary segmentation based on feature information, the red line segments represent the planned paths in the two-dimensional plane, and the purple points mark path endpoints. Regions 1 and 2 are the two displayed subregions of the same nose-frame flange. Their projected planning layouts are shown in Figure 9a and Figure 9b, respectively.

For the same region, the offset distance was set to the T-Scan 5's optimal working distance of 165 mm. The resulting three-dimensional path was loaded into the measurement scene, as shown in Figure 10. The red line indicates the planned scanning path for the nose-frame flange surface.

As shown in Figures 11 and 12, traditional algorithms tend to miss areas like A and B; meanwhile, the improved bidirectional row-scan path-planning algorithm performs noticeably better.



(**a**) (**b**)

Figure 9. Nose–frame edge panel–scanning path–planning results. (**a**) Region 01 planning results; (**b**) Region 02 planning results.

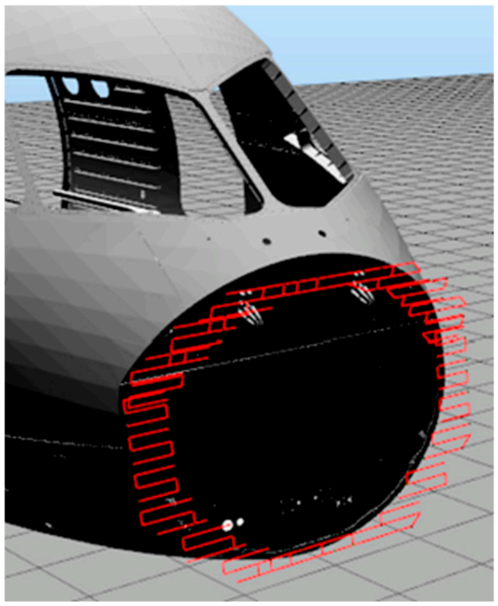
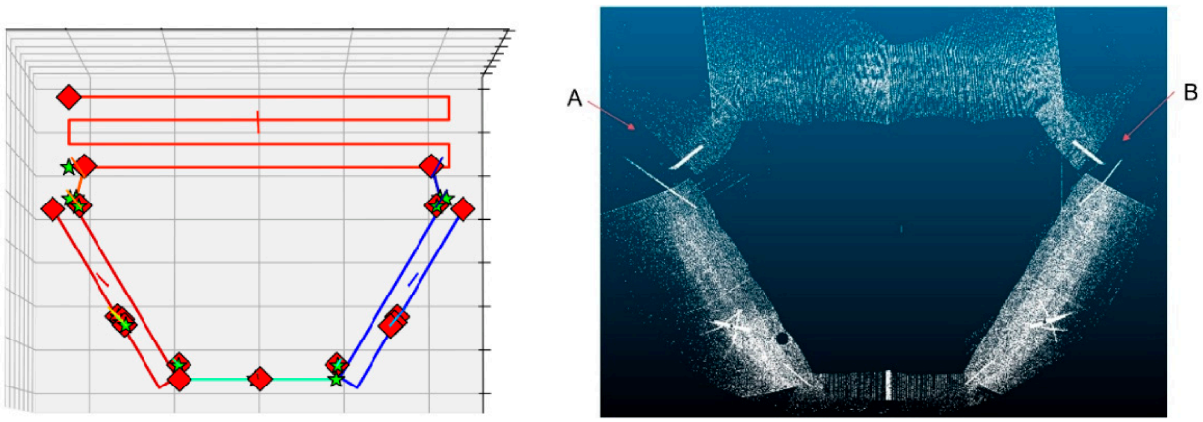
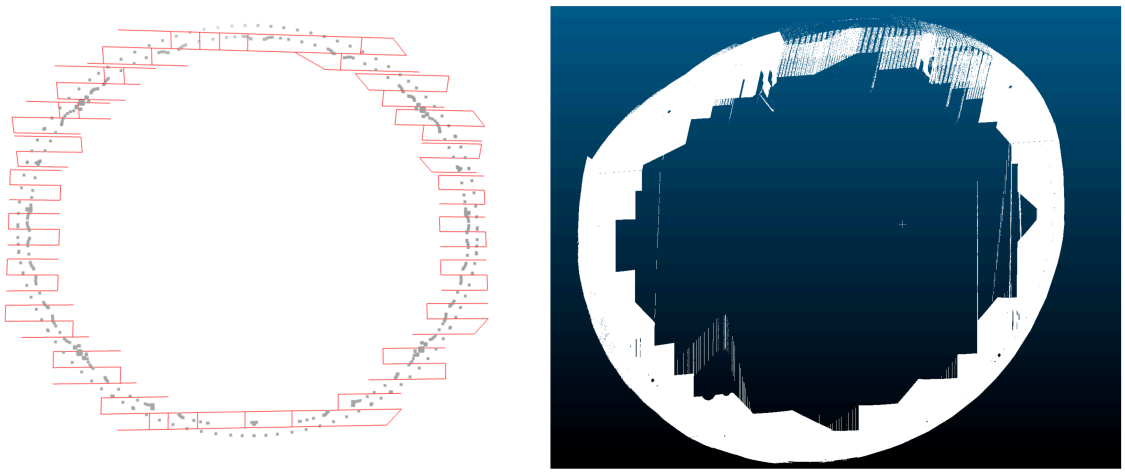


Figure 10. Three-dimensional path-planning results for the frame edge layout.



(**a**) (**b**)

Figure 11. Results of the original planning algorithm. (**a**) Scan path-planning results; (**b**) scan simulation results.



(**a**) (**b**)

Figure 12. Results of the improved scan path-planning algorithm. (**a**) Scan path-planning results; (**b**) scan simulation results.

Figures 11 and 12 illustrate the scanning-path planning and simulated coverage results obtained using the conventional bidirectional raster method and the proposed feature-aware method, respectively. The reference workflow discussed here uses bidirectional raster scanning without the feature-based secondary execution-cell selection introduced in the proposed workflow. In Figure 11a, red diamonds mark the key waypoints of the global path, including sub-region entrances/exits and inter-region connection nodes. Green pentagrams mark candidate connection endpoints of each sub-region, which are used for endpoint matching in the greedy global connection algorithm. Some key waypoints overlap spatially because one position bears multiple path node functions. Internal turning points of continuous scanning lines in the same sub-region are not marked separately as key waypoints.

As shown in Figure 11, the conventional method exhibits incomplete coverage in certain local feature regions, particularly near the transition areas of the nose-frame flange. In contrast, the proposed method incorporates feature-based secondary region partitioning to identify scanning execution units containing target feature points. By generating local scanning paths within these units, the proposed method provides additional scanning coverage in regions that are insufficiently covered by the conventional approach.

The calculated scanning coverage rate increases from 84% to 97%, representing an improvement of 13 percentage points. This result indicates that the proposed method improves the geometric coverage of target measurement features.

The proposed method prioritizes target-region coverage rather than minimum path length. The inclusion of additional scanning segments may increase the overall path length; therefore, the performance improvement is evaluated primarily in terms of scanning coverage and the completeness of target-feature measurement.

Quantitative comparison of the two methods is listed in Table 1.

4. Discussion

4.1. Limitations

The present study is limited to a geometric planning formulation and an illustrative example involving one aircraft nose-frame flange. The illustrative evaluation is restricted to one aircraft nose-frame flange. The two displayed regions belong to the same component and do not constitute independent geometric test cases. Applicability to substantially different curvatures, feature densities, and disconnected-region distributions has not been established.

The adopted partition dimensions have not been evaluated through sensitivity analysis. The treatment of partial boundary cells and sparse target features requires further investigation. Mean-normal offsetting does not guarantee pointwise measurement feasibility on curved surfaces, and the greedy connection procedure does not guarantee global optimality.

Robot-level reachability, joint limits, collision avoidance, singularities, and time-parameterized trajectory continuity have not been verified. The generated geometric paths therefore require further validation before practical execution.

4.2. Future Work

Future work will reconstruct a reproducible implementation and retain coordinate-level path outputs for quantitative benchmarking. Parameter sensitivity and additional geometries will be considered to assess robustness. Further evaluation will consider geometries with different curvature distributions, feature densities, and numbers of disconnected target regions. Future robot-level validation will draw on the distinction between geometric route generation and robot-executability checking demonstrated by Cristoiu et al. [24]. Their RoboDK-based application combines free-space graph planning with inverse-kinematics and robot-motion collision validation. For the present scanning task, future work will define complete scanner poses and tool and base transformations and evaluate joint limits, configuration continuity, collision status, and pointwise measurement constraints along both scanning and transfer motions. The cited study provides a methodological reference; the corresponding robot-level validation was not performed in the present study.

5. Conclusions

This study presents a feature-aware bidirectional raster path-planning method for robotic line-laser scanning of large components. The proposed approach integrates region growing, local planar projection, feature-based secondary partitioning, and greedy endpoint-based path organization to improve scanning coverage of spatially distributed target features.

A case study involving an aircraft nose-frame flange was conducted to evaluate the proposed method. Compared with conventional bidirectional raster scanning, the proposed method increased the calculated scanning coverage rate from 84% to 97%, corresponding to an improvement of 13 percentage points. The feature-based partitioning strategy enables scanning paths to be generated within execution units containing target feature points, thereby improving the completeness of geometric coverage in the selected measurement regions.

The results indicate that the proposed approach is effective in organizing scanning paths for complex components with dispersed target features. However, improved scanning coverage may require additional scanning segments and a longer overall trajectory. Further research will focus on evaluating the trade-off between scanning coverage and path length, as well as validating robot reachability, measurement constraints, and collision-free execution.

Author Contributions: Conceptualization, W.Z.; methodology, Z.G.; software, Z.G.; validation, J.L. and Z.G.; formal analysis, J.L.; investigation, J.L.; resources, L.H.; data curation, J.L.; writing—original draft preparation, J.L.; writing—review and editing, W.Z. and L.H.; visualization, J.L.; supervision, L.H.; project administration, L.H.; funding acquisition, L.H. All authors have read and agreed to the published version of the manuscript.

Funding: This work was supported by the MIIT Special Scientific Research Project on Civil Aircraft [MJZ3-4N22].

Data Availability Statement: The raw simulation data and code generated in this study are not publicly available due to project confidentiality restrictions. All results presented in the manuscript can be reproduced following the simulation settings and parameters described within the article.

Conflicts of Interest: The authors declare no conflict of interest.

References

1. Wang, Y.; Xie, H.; Deng, J.; Mao, J.; Li, W.; Zhang, H. Overview of key technologies for measurement robots in intelligent manufacturing. *J. Mech. Eng.* **2024**, *60*, 1–18. (In Chinese) [CrossRef]
2. Lin, J. Research on Measurement Trajectory Planning for Structural Components Based on Laser Scanning. Master's Thesis, Nanjing University of Aeronautics and Astronautics, Nanjing, China, 2019. (In Chinese)
3. Ai, X. Research on Scanning Path Planning in Aircraft Wing Assembly. Master's Thesis, Zhejiang University, Hangzhou, China, 2014. (In Chinese)
4. Zhao, A.; Wang, Z.; Wang, J. Scanning path generation based on aircraft panel features. *J. Nanjing Univ. Aeronaut. Astronaut.* **2021**, *53*, 344–349. (In Chinese)
5. Glorieux, E.; Franciosa, P.; Ceglarek, D. Coverage path planning with targetted viewpoint sampling for robotic free-form surface inspection. *Robot. Comput.-Integr. Manuf.* **2020**, *61*, 101843. [CrossRef]
6. Liu, Y.; Zhao, W.; Liu, H.; Wang, Y.; Yue, X. Coverage path planning for robotic quality inspection with control on measurement uncertainty. *IEEE/ASME Trans. Mechatron.* **2022**, *27*, 3482–3493. [CrossRef]
7. Jia, H.; Chen, H.; Chen, C.; Huang, Y.; Lu, Y.; Gao, R.; Yu, L. Research on path planning technology of a line scanning measurement robot based on the CAD model. *Actuators* **2024**, *13*, 310. [CrossRef]
8. Chen, C.; Jia, H.; Lu, Y.; Wu, A.; Zhang, X.; Lin, B.; Jiyan, Z.; Wang, X.; Yu, L. Research on the application of a dynamic programming method based on geodesic distance for path planning in Robot-Assisted laser scanning measurement of Free-Form surfaces. *Measurement* **2024**, *238*, 115317. [CrossRef]
9. Chen, H.; Huo, S.; Muddassir, M.; Lee, H.-Y.; Liu, Y.; Li, J.; Duan, A.; Zheng, P.; Navarro-Alarcon, D. PSO-based optimal coverage path planning for surface defect inspection of 3C components with a robotic line scanner. *IEEE Trans. Instrum. Meas.* **2025**, *74*, 7505012. [CrossRef]
10. Pi, J.; Zhang, Y.; Huang, X.; Yu, L.; Huang, N.; Zhu, L. Curvature-adaptive scanning path planning of robot optical measurement for large-scale freeform surfaces. *Robot. Comput.-Integr. Manuf.* **2026**, *100*, 103274. [CrossRef]
11. Sadaoui, S.E.; Mehdi-Souzani, C.; Lartigue, C.; Brahim, M. Automatic path planning for high performance measurement by laser plane sensors. *Opt. Lasers Eng.* **2022**, *159*, 107194. [CrossRef]
12. ShengQuan, F.; Qi, L.; JianXin, H.; Xiang, C. Posture planning method for complex feature measurement using a single-line laser scanner. *Appl. Opt.* **2023**, *62*, 9544–9552. [CrossRef] [PubMed]
13. Li, J.; Su, P.; Qu, L.; Lv, G.; Qian, W. A CAD-based method for 3D scanning path planning and pose control. *Aerospace* **2025**, *12*, 654. [CrossRef]
14. Gerbino, S.; Del Giudice, D.M.; Staiano, G.; Lanzotti, A.; Martorelli, M. On the influence of scanning factors on the laser scanner-based 3D inspection process. *Int. J. Adv. Manuf. Technol.* **2016**, *84*, 1787–1799. [CrossRef]
15. Mahmud, M.; Joannic, D.; Roy, M.; Isheil, A.; Fontaine, J.-F. 3D part inspection path planning of a laser scanner with control on the uncertainty. *Comput.-Aided Des.* **2011**, *43*, 345–355. [CrossRef]
16. Wang, Y.; Feng, H.-Y. Effects of scanning orientation on outlier formation in 3D laser scanning of reflective surfaces. *Opt. Lasers Eng.* **2016**, *81*, 35–45. [CrossRef]
17. Lin, X.; Wang, T.; Guo, L.; Li, L. Feature adaptive scanning path generation method for complex surfaces. *Infrared Laser Eng.* **2024**, *53*, 20240009. (In Chinese)
18. Gao, R. Research on Key Technologies for Automated Laser Scanning Measurement of Aircraft Skin Geometry. Master's Thesis, Nanjing University of Aeronautics and Astronautics, Nanjing, China, 2018. (In Chinese)
19. Guo, W.; Zhao, Z.; Ding, D.; Fu, Y. CAD-based path planning for line laser scanning of curved surface. *MM Sci. J.* **2021**, *2021*, 5259–5266. [CrossRef]
20. Xu, Z.; Guo, G.; Sun, Q.; Feng, G.; He, Y.; Xie, D. An improved region growing algorithm in 3D laser point cloud identification of rock mass structural plane. *Hydrogeol. Eng. Geol.* **2024**, *51*, 101–112. (In Chinese)
21. Wang, T. Assembly Positioning of Composite Structural Components Based on Measured Data. Master's Thesis, Changchun University of Science and Technology, Changchun, China, 2024. (In Chinese)
22. Zhang, H.; Fan, L.; She, Y.; Huang, J. Collision detection between power transmission lines and mechanical equipment based on airborne point clouds and monocular imagery. *Geotech. Investig. Surv.* **2024**, *52*, 59–64. (In Chinese)

23. Wang, Y.; Cai, L.; Lei, W.; Kou, P.; Liu, L.; Li, S. Design and implementation of palletizing and sorting path planning based on an improved greedy strategy. *J. Jianghan Univ. (Nat. Sci. Ed.)* **2024**, *52*, 43–51. (In Chinese)
24. Cristoiu, C.A.; Drăgoi, M.-V.; Nechita, R.-M.; Verdete, B.-M.; Dudici, C.L.; Cusma, C.N. Python Software Application for Obstacle-Avoiding Path Planning in RoboDK Using Free Space Graph and Robot Level Validation. *Appl. Sci.* **2026**, *16*, 4786. [CrossRef]

Disclaimer/Publisher's Note: The statements, opinions and data contained in all publications are solely those of the individual author(s) and contributor(s) and not of MDPI and/or the editor(s). MDPI and/or the editor(s) disclaim responsibility for any injury to people or property resulting from any ideas, methods, instructions or products referred to in the content.